energies

MDPI

Article

Experimental Study on the Thermal Performance of Flat Loop Heat Pipe Applied in Data Center Cooling

Yongle Tang [1,2], Xuewei Zhang [2] and Zhichun Liu [1,*]

[1] School of Energy and Power Engineering, Huazhong University of Science and Technology, Wuhan 430074, China; tangyl0518@163.com
[2] Guangdong Shenling Environmental System Co., Ltd., Foshan 528313, China
* Correspondence: zcliu@hust.edu.cn

Abstract: The cooling system is the auxiliary equipment that consumes the most energy in a data center, accounting for about 30 to 50% of the total energy consumption. In order to effectively reduce the energy consumption of a data center, it is very important to improve the heat exchange efficiency at the chip level. Compared with air cooling, single-phase cold plate liquid cooling, and immersion liquid cooling, the flat loop heat pipe (FLHP) is considered to be a better chip-level cooling solution for data centers. It has extremely high heat transfer efficiency and heat flux variability, and it can avoid the operation risk caused by liquid entering the server. In this paper, a FLHP with an evaporator designed with a "Tesla valve" flow channel configuration is developed. Experiments on the FLHP are carried out, focusing on the installation angles and cooling condition factors. The results show that an inclination angle of 20° is the critical point of the influence of gravity on the performance of the FLHP; to ensure good operation of the FLHP, the installation angle should be greater than 20°. The equivalent heat transfer coefficients of the FLHP condenser under different cooling conditions are calculated. It is found that water cooling can provide higher cooling heat transfer coefficients with lower energy consumption and operating noise. Additionally, the heat transfer limit, operating temperature uniformity, and start-up stability of the FLHP are significantly improved under water cooling conditions. The maximum heat load of the FLHP is up to 230 W, and the temperature difference of the evaporator surface can be controlled within 0.5 °C, under 20 °C water cooling. Finally, using the FLHP for thermal management of the chip, its heat transfer efficiency is 166 and 41% higher than that of air cooling and water cooling, respectively.

Keywords: data center; chip-level cooling solution; FLHP; installation angle; cooling conditions

Citation: Tang, Y.; Zhang, X.; Liu, Z. Experimental Study on the Thermal Performance of Flat Loop Heat Pipe Applied in Data Center Cooling. *Energies* **2023**, *16*, 4677. https://doi.org/10.3390/en16124677

Academic Editor: Gabriela Huminic

Received: 17 May 2023
Revised: 7 June 2023
Accepted: 11 June 2023
Published: 13 June 2023

1. Introduction

Nowadays, the data center has become a core member of the electronic information industry. With the rapid development of 5G mobile communication, the Internet of Things, cloud computing, big data, artificial intelligence, and other applications, the construction scale and number of data centers are expanding [1]. According to the report, by the end of the third quarter of 2019, there were 504 hyperscale data centers [2] in the world, and this number will grow by 12–14% per year in the next five years [3]. The energy consumption of a data center is 40 times that of a typical office building [4]. In 2020, the energy consumed by data centers accounted for 1–2% of the world's total electricity consumption [5,6]. In the UK, data centers accounted for 1.5% of annual electricity consumption in 2016, and this value increased to 20% by 2020 [7]. In China, the total electricity consumption of data centers reached 160.8 billion kWh in 2018, exceeding the total electricity consumption of the entire city of Shanghai [8]. The total energy consumption resulting from the rapid development of data centers is increasing, which has become a major challenge for data centers development. Therefore, improving the energy efficiency level of data centers and promoting energy conservation and emission reduction in data centers is the key to ensuring its sustainable development.

The data center cooling system provides a suitable temperature and humidity environment to ensure the efficient and stable operation of IT equipment, power supplies, batteries, and other equipment in the data center. Thus, it consumes a lot of electricity, accounting for about 30 to 50% of the total energy consumption of the data center [9–11]. Cooling systems are the most energy-consuming auxiliary equipment in a data center. Therefore, reducing the energy consumption of cooling systems is the key to improving the energy utilization efficiency of data center. There are two main ways to reduce the energy consumption of data center cooling systems. One aspect is to improve the cooling efficiency or the performance of the air conditioning system [12,13]. Another aspect is to make full use of a natural cold source and increase its utilization time. Making full use of natural cooling sources is closely related to the heat transfer efficiency of a cooling system. If the heat transfer efficiency between the chip heat source and the outdoor cold source can be improved, the selection range of the natural cooling source will be wider, and the available time will be longer. Consequently, the energy consumption of data centers can be further reduced. It is worth noting that improving the heat transfer efficiency of the cooling system needs to focus on the front section of the heat transfer chain, that is, the chip section. This is because the chip section exhibits the highest heat flux density, which easily leads to heat transfer loss.

Currently, the chip-level cooling solutions commonly used in data centers include air cooling and liquid cooling [14,15]. Air cooling uses a fan inside the server to force the low-temperature airflow into the server cabinet. The high-speed airflow passes over the surface of the chip to complete the heat absorption and transfer. It is the most widely used cooling solution in data centers [16,17]. In the air cooling solution, the rotational speed of the built-in fan in the server can be intelligently adjusted to match the cooling capacity required under different loads, thereby saving energy consumption. For example, a monitoring device could be introduced to monitor the server inlet air temperature and the temperature of the internal heating element. However, due to the low density and low heat dissipation capacity, air cooling is a cooling solution with low efficiency. Its maximum heat dissipation capacity is about 37 W/cm^2 [18], which is only suitable for cooling data centers with a single rack power of 10–15 kW; note that the power of the blade server can easily exceed 60 KW [19]. As an alternative to the practical limitations of air cooling, the liquid cooling solution has attracted attention. The heat dissipation of liquid cooling can be as high as 202 W/cm^2, which is about six times that of traditional air cooling [20]. It can be divided into indirect liquid cooling and direct liquid cooling. Indirect liquid cooling is a heat dissipation process where there is no direct contact between the heat source and the coolant. Usually, the low-temperature liquid is introduced into the sealed metal cavity, and the heat released by the heat source is absorbed by the convective heat exchange based on the flow of the liquid. In a liquid cooling system for data centers, the low-temperature liquid is supplied from a coolant distribution unit (CDU) to the closed liquid circuit inside the server for CPU heat dissipation [21]. Since the thermophysical properties of liquids are much higher than that of air, the liquid cooling method can use a higher cooling temperature to realize the thermal management of the chip, which provides the feasibility to further reduce energy consumption [22]. A cold plate is the most common type of indirect liquid cooling radiator. The key to determining the heat transfer performance of a cold plate lies in its structure and the cooling medium used. Currently, researchers are focused on the structural design of microchannel heat sinks and their enhanced heat transfer performance. Compared with traditional cold plates, the heat transfer performance of microchannels is superior [23,24]. The core of the research is the pressure drop, coolant flow rate, inlet and outlet temperature, required pumping power, heat transfer coefficient, and other parameters of microchannel radiators with different structures [25,26]. However, there are two disadvantages of indirect liquid cooling: the potential risk of leakage and the specific size requirements for the system layout [27]. Direct liquid cooling technology can overcome the above problems. An insulating liquid is used as the cooling medium for direct liquid cooling, which is in contact with the surface of the heating chip directly to efficiently

realize the thermal management of the heat source [28,29]. Generally, the heat transfer efficiency of two-phase immersion liquid cooling can be improved by special treatment or structural modification of the heat transfer surface, such as increasing its roughness or increasing the heat transfer surface area. It should be noted that electronic components or the entire server need to be immersed in a cabinet filled with a large amount of cooling liquid for immersion liquid cooling. It means that this solution has higher requirements on the thermophysical properties of the cooling liquid.

Three common chip-level cooling methods for data centers are reviewed above, but they all have significant shortcomings. The heat transfer efficiency of air cooling is too low to be applied to the cooling of high heat flux chips. For single-phase cold plate liquid cooling, the liquid needs to be imported into the server, resulting in a risk of leakage. Furthermore, the heat transfer efficiency of single-phase liquid is lower than that of the phase change process. The high requirements for the coolant and the overall construction cost for immersion liquid cooling are much higher than other solutions.

Significantly, heat pipes utilize the gas–liquid phase change process of the working fluid in the tube to complete heat transfer, showing extremely high heat transfer efficiency. The use of heat pipe technology can effectively avoid the risk of cooling-liquid leakage inside the server. In addition, the heat pipe is a passive heat transfer element without rotating parts and additional drive devices, which means that it has extremely high reliability [30]. Thus, heat pipe technology is promising for chip-level cooling in data centers [31]. Currently, it is widely used in the heat dissipation of high heat flux electronic components, such as notebooks, mobile phones, digital cameras, etc. [32]. On the other hand, it is also widely used in the cooling of the mainframe CPU of a personal computer, and the heat dissipation effect of air-cooled radiators is improved by embedding the heat pipe into the bottom plate or fin of the air-cooled radiator [33]. The factors that affect the thermal performance of heat pipes mainly include capillary core structure, working fluid filling rate, etc. [34].

The common integrated heat pipe has a simple structure. However, due to the limitation of heat transmission distance and the orientation of cold and heat sources, it is difficult to apply common heat pipes to chip cooling in data centers. At this time, loop heat pipes, especially the flat-plate loop heat pipe (FLHP) with the evaporator in close contact with the chip surface, can complete the thermal management for data center chips more efficiently and reliably. Generally, the interior of the evaporator of a FLHP has a capillary structure. This structure divides the evaporator cavity into upper and lower layers, which are liquid channels and vapor channels, respectively [35,36]. Note that this type of structure is not conducive to the ultra-thin development trend of the FLHP. Therefore, FLHPs in which the evaporator cavity is separated by a wick structure into the left and right spaces have been developed [37,38]. The left and right spaces correspond to the vapor channels' space and liquid storage chamber, respectively. The vapor channels are always parallel flow channels. Unfortunately, this structure leads to the excessive flow resistance of the liquid in the wick structure, thereby weakening the heat transfer limit of the FLHP. However, if the liquid reservoir is not separated from the vapor flow area by a wick structure, the misdirected flow of vapor will cause unstable operation of the FLHP [39]. To make matters worse, some vapor will flow back to the liquid pipeline, causing back heat leakage. The counter-flowing vapor will collide with the returning condensate, resulting in an increase in the pressure drop of the circulation of the working fluid. Inevitably, the above phenomena will lead to a sharp drop in the performance of the FLHP.

In general, the FLHP performs best when its condenser is installed vertically above the evaporator. However, as the compactness of data center cabinets increases, the installation space of the FLHP will be strictly limited. At this time, the working inclination angle of the FLHP becomes an important parameter affecting its performance. In addition, the cooling conditions on the condensing side of the FLHP also need to match the cooling system of the data center. This requires adjusting the cooling conditions to take advantage of the natural cooling source as much as possible to find the best operating conditions for the system. In this work, a new type of FLHP for the chip-level cooling of a data center is

developed. The internal design of the FLHP evaporator is a micro-channel with a "Tesla valve" configuration, which facilitates the stable operation of the FLHP and reduces back heat leakage. The effects of the working inclination angle and cooling conditions, including cooling heat transfer coefficient and cooling temperature, on the thermal performance of the FLHP are experimentally investigated.

2. Experimental Set-Up

2.1. FLHPs Prototype

The FLHP prototype developed in this study uses oxygen-free copper as the shell material and deionized water as the working fluid. The schematic diagram and image of the FLHP sample are shown in Figure 1. The composition of the FLHP includes an evaporator, condenser, gas–liquid pipeline, and other components. Detailed parameters of the FLHP are listed in Table 1. The evaporator contains a capillary core structure and a support column, and the capillary core structure adopts sintered copper powder. There are two blank areas between the left and right edges of the capillary core structure and the two sides of the metal substrate, which are used as the gas collection space and the liquid storage space of the FLHP. A fixed gap is left between the sintered copper powder capillary core and the support column to form a microchannel for the flow of working fluid, with a width of 1 mm and a height of 3 mm. A special circuit design is applied to process the microchannel, which has the configuration feature of a "Tesla valve", as shown in Figure 2. It is formed by the interlaced connection of multiple arc-shaped channels and straight-line channels, and each circuit has a "T"-shaped bifurcation and a "Y"-shaped intersection. When the working fluid flows through the microchannel from right to left (forward flow), it will be divided into two paths at the "T" bifurcation. After that, most of the fluid will pass through the circuit along the straight main channel, and a small part of the fluid will enter the arc channel. Finally, the two channels of fluid will converge at the "Y"-shaped intersection, and the flow of fluid will be accelerated. On the other hand, when the fluid flows from left to right, it is defined as a reverse flow pattern. In this case, the flow will split at the "Y" junction. Afterwards, most of the flow will proceed into the arc-shaped flow channel along the original flow direction at a relatively high speed, and its speed will gradually decrease. The remaining small amount of fluid will pass through the straight flow channel and meet the fluid of the arc flow channel at the "T" bifurcation. Since the two streams of fluid at the intersection flow in opposite directions, the flow of fluid will face enormous resistance. Based on this structural design, the steam generated by the evaporator can be ensured to flow spontaneously from right to left, thus, avoiding the steam entering the liquid storage chamber. It is beneficial to reduce the "backward" heat conduction of the evaporator and promote the directional and stable operation of the loop heat pipe.

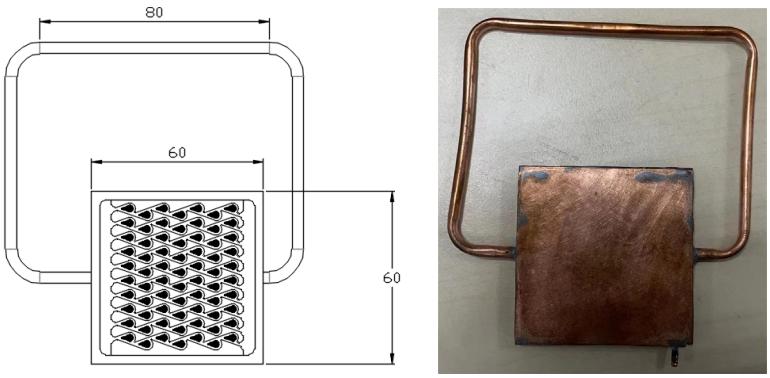

Figure 1. The schematic and physical drawings of the FLHP.

Table 1. Structure parameters of the FLHP.

Parameters	Value	Parameters	Value
Evaporator size (mm)	60 × 60 × 5	Condenser length L (mm)	80
Loop pipe outer diameter d_o (mm)	4.0	Condenser external surface area A_{hp} (mm^2)	1.0048
Loop tube inner diameter d_i (mm)	3.6	Mass filling of working fluid m (g)	4.0

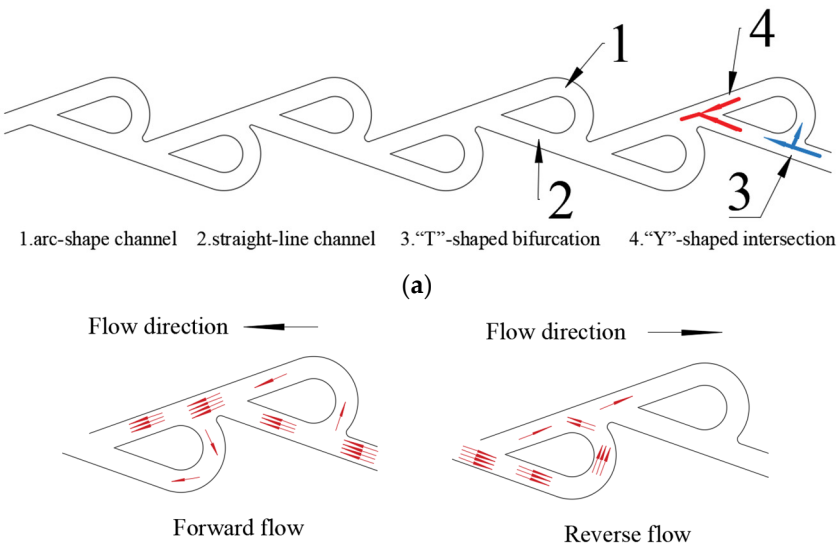

Figure 2. The structure of the "Tesla valve". (**a**) Schematic diagram of the "Tesla valve". (**b**) Schematic diagram of forward and reverse flow patterns in the "Tesla valve".

2.2. Experimental Device

In order to fully test the heat transfer performance of the FLHP, two different cooling methods are adopted for the condensing end of the FLHP to evaluate the influence of cooling conditions on the performance of the FLHP, namely air cooling and water cooling. According to the experimental devices required by different cooling methods, two FLHP performance test platforms are built, as shown in Figures 3 and 4. Both platforms include four modules: a heating module, a data acquisition module, a heat preservation module, and a cooling module. Except for the difference in the cooling module, the rest of the two platforms are the same.

2.2.1. Air Cooling Experiment

The heating module in the experiment is composed of a DC-stabilized power supply, a ceramic heating rod, and a copper plate. The surface size of the copper plate is 40 mm × 40 mm, and the copper plate includes a base. A ceramic heating rod is embedded in a copper plate base. During the experiment, the heating rod is energized by a DC-stabilized power supply, and then the heating rod heats the surface of the copper plate to simulate the heating state of the server chip. The data acquisition module and thermocouples K-OMEGA (with an accuracy of ±0.5 °C) are used to measure the temperature on the surface of the heat pipe evaporator, the inlet and outlet of the evaporator, and the inlet and outlet of the condenser. Nine temperature measurement points are arranged, as shown in Figure 3. Finally, the thermal signals collected by the thermocouples will be fed back to the computer, and the temperature changes at each point are displayed in real-time for subsequent experimental analysis. The thermal insulation device of the test platform includes a bakelite base and thermal insulation cotton. The heating copper plate used in

the experimental heating is fixedly placed on the bakelite base. During the experiment, the FLHP evaporator is closely attached to the surface of the heating copper plate, and thermal silica gel is applied between the two to reduce the contact thermal resistance. In order to reduce heat leakage, all surfaces except the condenser area are tightly wrapped with thermal insulation cotton.

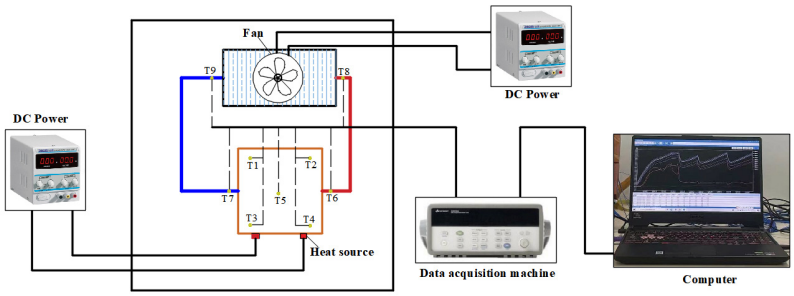

(**a**)

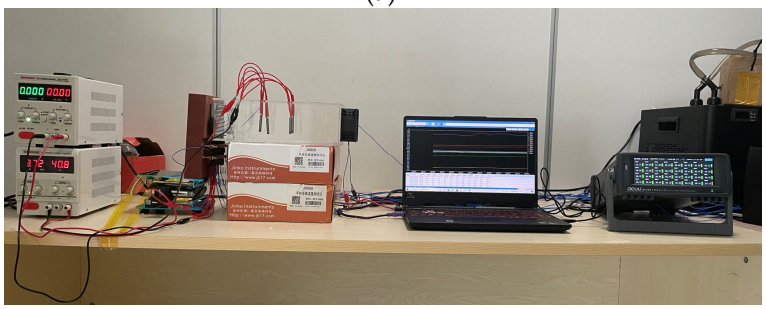

(**b**)

Figure 3. Introduction of the air-cooling experimental set-up. (**a**) Schematic diagram of the air-cooling experimental system. (**b**) Experiment platform of the air-cooling.

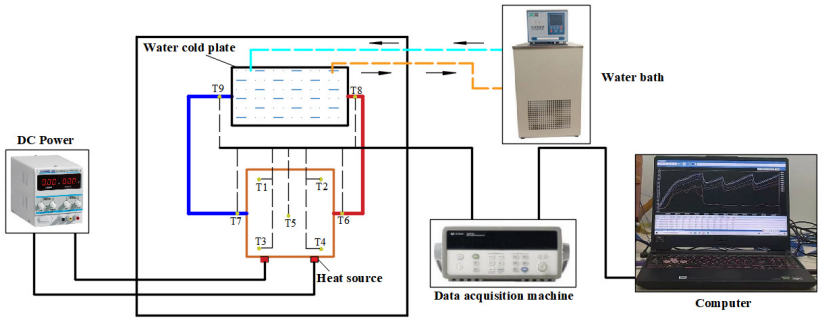

(**a**)

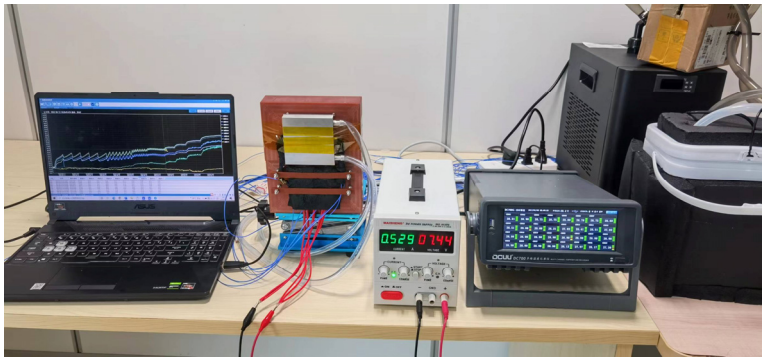

(**b**)

Figure 4. Introduction of the water-cooling experimental set-up. (**a**) Schematic diagram of the water-cooling experimental system. (**b**) Experiment platform of the water-cooling.

The cooling devices used in different cooling methods are varied. In the air-cooling experiment, in order to improve the air-cooled heat transfer capacity of the FLHP condenser, an aluminum fin module with a size of 80 mm × 80 mm × 35 mm is customized. The bottom of the module is slotted and fits with the FLHP condenser pipeline. Afterwards, an air duct with a cross-section of 80 mm × 80 mm and a length of 400 mm is built with acrylic boards. The end of the air duct is aligned with the air-cooled fin module, and a DC fan is installed at the head of the air duct. The fan is powered by a DC-stabilized power supply to generate high-speed airflow with different air volumes. Further, in order to better adjust the temperature of the cooling airflow, four ceramic heating rods are arranged along the air duct, and thermocouples monitor the temperature at the end of the air duct.

During the experiment, the input heating power is controlled by adjusting the DC-stabilized power supply. At the beginning of the experiment, an initial power will be set, such as 10 W. When the temperature of each point on the surface of the evaporator reaches a steady state under the current power, the input heat load is gradually increased at intervals of 10 W. When a sudden rise in the surface temperature of the evaporator is detected, that is, the FLHP reaches the heat transfer limit, the experimental test is ended. In addition, when the surface temperature of the FLHP evaporator exceeds 70 °C, the test will be stopped, even if there is no sudden increase in temperature.

2.2.2. Water Cooling Experiment

The composition of the water-cooling experimental platform is similar to that of the air-cooling experiments, with only differences in the cooling methods and corresponding equipment. In order to improve the heat exchange capacity of the FLHP condenser, a water-cooled heat dissipation module with a size of 80 mm × 80 m × 15 mm is customized. Similarly, the groove at the bottom of the module fits with the FLHP condenser pipe to achieve indirect water cooling of the FLHP condenser. Inside the module, a channel with an inner diameter of 8 mm and a total length of 434 mm is processed in a serpentine shape. Both ends of the channel are respectively connected to the inlet and outlet of the cooling water. During the experiment, cooling water at a fixed temperature is provided by a constant temperature water bath. The parameter measurement settings in the water-cooling experiments are consistent with those in the air-cooling experiments.

2.3. Uncertainty of the Measurement

In this study, the detected parameters include temperature T, cooling water flow Q_w, DC power output power P (used to provide a simulated heat source and control fan speed). The measurement uncertainties of the above parameters are calculated according to the following methods.

(1) Measurement uncertainty of temperature T

According to the "National Metrology Technical Specifications of the People's Republic of China JJF1059-2012" [40], the required measurement parameters are repeatedly tested under the same conditions to ensure the repeatability and validity of the experimental results. The parameter (temperature, T) that can be directly measured in the experiment and its uncertainty is calculated using the type A uncertainty analysis method. Its calculation formula is $U(T_i) = \sqrt{\frac{1}{I(J-1)}\sum_{j=1}^{J}\sum_{i=1}^{I}(T_{ij} - \overline{T_i})}$, where i is the serial number of the tested temperature point, and j is the serial number of the repeated experiment. Based on the tested results, the maximum deviation of the temperature T measured by the thermocouple is 1.73 °C, and the corresponding maximum uncertainty is 2.81%.

(2) Measurement uncertainty of cooling water flow Q_w

The cooling water flow is controlled by adjusting the opening of the flow valve, and the flow is monitored by a turbine flowmeter. The uncertainty caused by the instruments is analyzed by B type uncertainty analysis method, which is calculated by the formula $U(E) = \frac{A}{k}$. Among them, A is the nominal error obtained from the instrument manual,

and the value of k is $\sqrt{3}$. In this work, the nominal error of the turbine flowmeter is $\pm 1.5\%$, and the standard uncertainty of cooling water flow Q_w can be calculated as $U(Q_w) = 1.5\%/\sqrt{3} = 0.866\%$.

(3) Measurement uncertainty of DC power output power P

Both the simulated heat source and fan power in this work are supplied by a DC-regulated power supply. The instrument causes the uncertainty of the DC power supply, and the nominal error of the DC power supply used is 1%; then the standard uncertainty of the voltage can be calculated as $U(V) = 1\%/\sqrt{3} = 0.577\%$. Based on the principle of error transfer, the uncertainty of the output power P of the DC power supply can be calculated as $U(P) = \frac{\sqrt{(I \cdot u(V))^2 + (V \cdot u(I))^2}}{V \cdot I} = 2.341\%$.

3. Results and Discussion

3.1. Effect of Tilt Angles on the Thermal Performance

Due to the limitation of installation space, the FLHP may have different installation angles in practical applications. Generally speaking, the condenser of the FLHP is located above its evaporator, which is conducive to the circulation of the internal working fluid. This is because the reflow direction of the condensate is consistent with the direction of the gravity field. As the FLHP is gradually placed horizontally, the auxiliary function of gravity is gradually weakened. When the condenser and evaporator are at the same level, gravity will not help the condensate reflux. However, more installation space is always required to achieve a vertical installation of the FLHP. It will sacrifice the overall compactness of the system. Therefore, it is of great significance to find the balance point between the installation angle and FLHP performance and to determine the most cost-effective installation angle.

3.1.1. Operating Characteristics

This section explores the gravity effect on the FLHP under an air-cooling condition. Six different tilt angles were measured, from 0° to 90°. The temperature curves of the FLHP under various heat loads at each inclination angle are shown in Figure 5. It can be found that the FLHP can start with 10 W heating power at all inclination angles. The threshold of the start-up temperature of the FLHP is relatively high at a small angle, and the temperature will drop obviously when it achieves the threshold. This is mainly due to the weak effect of gravity on promoting condensate return at small angles. The longer residence time and slower reflow rate of the working fluid in the condensing section lead to heat accumulation and temperature rise in the evaporator.

When the FLHP starts up completely, there will be no significant temperature drop with the increase of heat load. As the heat load continues to increase, the surface temperature of the evaporator responds quickly and rises sharply. Then, the thermal equilibrium is quickly re-established and the temperature remains stable. Compared with high heat load, the FLHP is less stable in operation at low heating power, showing obvious temperature fluctuations.

Observing the operating curves of the FLHP at different inclination angles, the operating characteristics before and after the inclination angle of 20° show very significant differences. The temperature rise of the FLHP with the increase of heat load at a small tilt angle is huge. The upper-temperature limit of 70 °C will be reached quickly. The maximum heat transfer capacity at 0° and 10° operating angles are 30 W and 70 W, respectively. When the operating angle reaches 20°, the heat transfer limit of the FLHP can reach 120 W. Unfortunately, as the inclination angle continues to increase up to 90°, its heat transfer limit only increases by 10 W compared to that at 20°. It can be concluded that the inclination angle of 20° is the critical performance point of the FLHP, and it is also the most cost-effective operating angle.

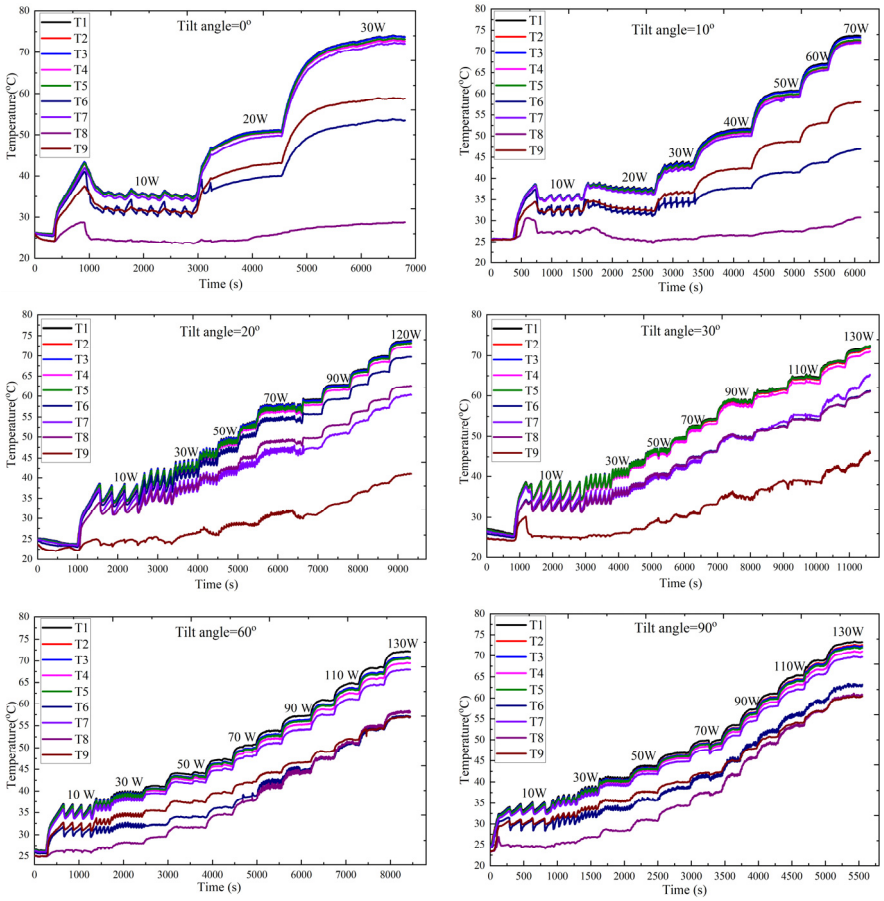

Figure 5. The operating temperature curve of the FLHP at various tilt angles.

3.1.2. Evaporator Temperature and Thermal Resistance

Furthermore, working temperature and thermal resistance are important indexes to evaluate the heat transfer performance of the FLHP. The effect of the operating angle on the heat transfer performance of the FLHP can be further clarified by these two indexes. The evaporator temperature and thermal resistance can be calculated by Equation (1) and Equation (2), respectively. T_c is the average temperature of the condenser, which is the average value of the inlet and outlet temperatures of the condenser. Q_{heat} is the input heat load.

$$T_e = \frac{T_1 + T_2 + T_3 + T_4 + T_5}{5} \quad (1)$$

$$R = \frac{T_e - T_c}{Q_{heat}} \quad (2)$$

From Figure 6a, it can be found that when the angle changes from 0° to 20°, the temperature of the evaporator drops sharply, indicating that the effect of gravity assisting working fluid circulation is quite remarkable. That is, a slight change in angle can lead to a significant performance improvement of the FLHP. From 20° to 90°, the increase of the inclination angle of such a large span brings only a 10 W increase in the heat transfer capacity, and the evaporator temperature has no obvious difference under each heat load. Especially after the angle exceeds 60°, the temperature curves of each operating point basically coincide, which indicates that the increase of gravity can no longer promote the circulation rate of the working fluid. Based on its own capillary force, it is sufficient to quickly reach a thermal equilibrium of the FLHP under various heat loads with the aid of gravity force under the condition of 30° inclination. At this time, the working temperature of the FLHP is determined not by the refrigerant cycle's driving force but by

the condenser's heat dissipation rate. Therefore, under the same cooling condition, the working temperature of the FLHP after the tilt angle exceeds 30° is very close.

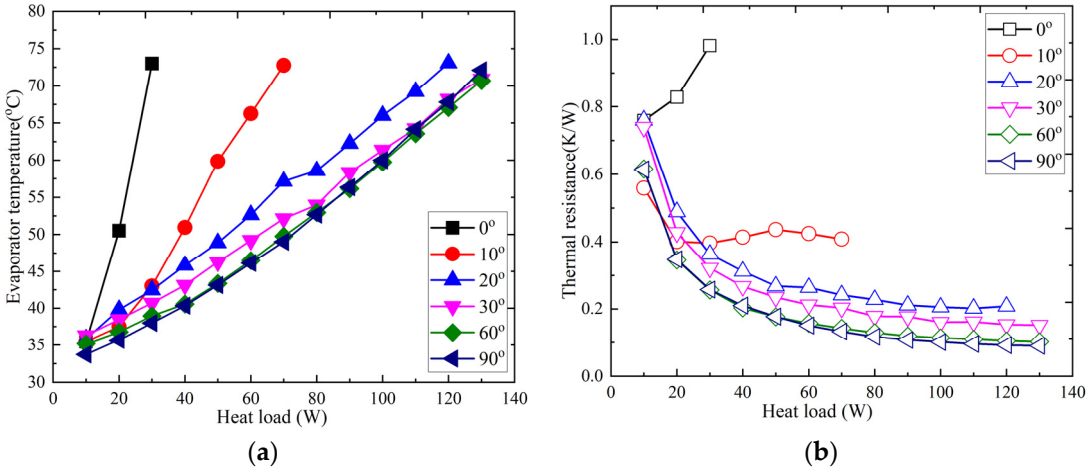

Figure 6. Variation of evaporator temperature and thermal resistance with heat load under various tilt angles. (**a**) Evaporator temperature. (**b**) Thermal resistance.

In combination with the thermal resistance curve of the FLHP shown in Figure 6b, it can be found that the driving force of the working fluid cycle is seriously insufficient at a 0° inclination angle. At this time, the thermal resistance curve shows a sharply rising trend, indicating that the circulating flow rate of the working fluid cannot transfer the current heat load completely. The heat accumulates continuously at the input and the evaporator temperature rapidly. At a heat load of 30 W, the evaporator temperature of the FLHP exceeds 70 °C, reaching the test limit of this experiment. When the tilt angle increases to 10°, the FLHP exhibits smaller thermal resistance. The thermal resistance decreases slightly with the increase of heat load and finally stabilizes at about 0.4 K/W. After an inclination greater than 20°, the FLHP has been able to maintain a smooth cycle in its working fluid. In this situation, increasing the heat load will cause the liquid film in the evaporator to become thinner, thereby improving the heat transfer efficiency of evaporation. Although the heat input to the evaporator is increasing, it can be transferred to the condenser in time by the internal working fluid circulating inside the FLHP. As a result, the overall thermal resistance of the FLHP will continue to decline. It should be noted that the thermal resistance of the FLHP still decreases slightly with increasing tilt angle in the range of 20° to 90°. At the same heat load, the temperature difference between the evaporator and the condenser is the key to determining the thermal resistance. As shown in Figure 6a, the evaporator temperature at a 20° tilt angle is slightly higher than that at the last three angles. More importantly, the outlet temperature of the FLHP condenser increases significantly with increasing tilt angle. The reason for the increase in the outlet temperature of the condenser is that the condensed liquid will not accumulate in the horizontal section of the condenser, so it will not be overcooled. The higher condenser outlet temperature reduces the temperature difference between the condenser and the evaporator, and as a result the thermal resistance decreases with the increase of tilt angle.

3.2. Effect of the Cooling Condition on the Thermal Performance

3.2.1. Effect of the Cooling Heat Transfer Coefficient

In this work, two cooling methods were used to cool the FLHP, namely forced air cooling and indirect water cooling. The heat exchange principles and heat transfer paths of the two cooling methods were different. The heat on the condenser of the FLHP mainly comes from the latent heat released during the condensation process of the gas-phase working fluid in the tube. The heat will first be transferred from the inner wall of the copper tube to the outer wall by heat conduction. Afterwards, for different cooling methods, the

path of heat transfer was found to change. For air cooling, the heat is transferred from the outer wall of the FLHP condenser to the base of the heat dissipation module by thermal conduction. The heat dissipation module is in close contact with the outer wall of the FLHP condenser, and then, the heat gradually diffuses to the fin surface of the module. Finally, heat is transferred to the air by thermal convection by the high-velocity airflow passing over the surface of the fins. On the other hand, for water cooling, the heat from the outer wall of the FLHP condenser will be transferred to the base of the water-cooling plate contacted with it. Then, it is further transferred to the inner wall surface of the serpentine pipe inside the water-cooling plate. Finally, the heat transfer is realized by thermal convection of the low-temperature liquid flowing in the tube.

Based on the heat transfer process, the air-cooling heat transfer coefficient between the fin surface and the flowing air and the water-cooling heat transfer coefficient of the liquid flow in the water-cooling plate can be calculated, respectively.

The first is the calculation of the air-cooling heat transfer coefficient. The structure parameters of the air-cooling module are shown in Table 2. According to the parameters in the table, the convective heat transfer coefficient of forced air cooling on the fin surface can be calculated, and the formulas are referenced from [41].

Table 2. Structure parameters of the air-cooling module.

Parameters	Value	Parameters	Value
Air module length L_a (mm)	80	Net face ratio ξ	0.63
Air module width W_a (mm)	80	Wall area between the fins A_1 (mm^2)	0.004032
Air module thickness t_a (mm)	5	Fin surface area A_2 (mm^2)	0.0504
Fin thickness t_f (mm)	0.9	Total area A_{to} (mm^2)	0.054432
Fin spacing δ (mm)	2.4	Air-specific temperature T_a (°C)	25
Number of fins N	21	Air thermal conductivity λ_a (W/m·°C)	0.02622
Fin height h_f (mm)	30	Fin thermal conductivity λ_f (W/m·°C)	205
Air Prandtl number Pr_a	0.7	Air kinematic viscosity ν_a (m^2/s)	1.54×10^{-5}

Air velocity in minimum cross section:

$$v_{max} = v/\xi \tag{3}$$

Reynolds number:

$$Re_a = v_a \cdot D/\nu_a \tag{4}$$

Nusselt number:

$$Nu_a = 0.037({Re_a}^{0.8} - 850){Pr_a}^{1/3} \tag{5}$$

Air convection heat transfer coefficient:

$$\alpha_0 = Nu_a \cdot \lambda_a/h_f \tag{6}$$

Fin efficiency:

$$\eta_f = \mathrm{th}(mH')/mH' \ (m = \sqrt{\frac{2\alpha_0}{\lambda_f t_f}}, \ H' = h_f + t_f/2) \tag{7}$$

Overall fin surface efficiency:

$$\eta_t = (A_1 + \eta_f \cdot A_2)/A_{to} \tag{8}$$

Air cooling heat transfer coefficient:

$$\alpha_a = \alpha_0 \cdot \eta_{to} \tag{9}$$

Then the water-cooling heat transfer coefficient can be calculated. The structure parameters of the water-cooling module are shown in Table 3. The convective heat transfer coefficient of the water flowing through the channel of the module can be calculated according to the parameters in the table.

Table 3. Structure parameters of the water-cooling module.

Parameters	Value	Parameters	Value
Water module length L_w (mm)	80	Liquid channel internal surface area of A_w (mm^2)	0.011
Water module width W_w (mm)	80	Module thermal conductivity λ_m (W/m·°C)	205
Water module thickness T_w (mm)	15	Cooling water specific temperature t_w (°C)	25
Liquid channel inner diameter d_{wi} (mm)	8	Cooling water kinematic viscosity ν_w (m^2/s)	1.006×10^{-6}
Liquid channel cross-sectional area A_{cross} (mm^2)	5.02×10^{-5}	Cooling water thermal conductivity of λ_w (W/m·°C)	0.599
Liquid channel total length L_{wt} (mm)	434	Cooling water Prandtl number water Pr_w	7.02

Cooling water velocity:

$$v_w = \frac{Q_w}{1000 \times 60 \times A_{cross}} \tag{10}$$

Reynolds number:

$$Re_w = v_w \cdot d_{wi} / \nu_w \tag{11}$$

Nusselt number:

$$Nu_w = 0.023 {Re_w}^{0.8} \cdot {Pr_w}^{0.4} \tag{12}$$

Air cooling heat transfer coefficient:

$$\alpha_w = Nu_w \cdot \lambda_w / d_{wi} \tag{13}$$

In order to directly compare the difference between the air-cooling and water-cooling heat transfer coefficients, the heat transfer coefficients under different cooling conditions are converted into the equivalent heat transfer coefficient of the outside tube of the FLHP condenser. The equivalent heat transfer coefficient is based on the external surface area of the tube of the FLHP condenser. The concrete transformation relations are shown as Equations (14) and (15). The outside tube equivalent heat transfer coefficients of the FLHP condenser under different cooling conditions are shown in Table 4.

Air cooling:

$$\alpha_{hp} = \left(\frac{\delta_a}{\lambda_f} + \frac{A_{hp}}{A_a \cdot \alpha_a}\right)^{-1} \tag{14}$$

Water cooling:

$$\alpha_{hp} = \left(\frac{\delta_w}{\lambda_m} + \frac{A_{hp}}{A_w \cdot \alpha_w}\right)^{-1} \tag{15}$$

The equivalent heat transfer coefficients of the FLHP condenser under different operating conditions were calculated. Furthermore, the performance of the FLHP under different cooling heat transfer coefficients were analyzed. Figure 7a shows the variation of the evaporator temperature of the FLHP with the cooling heat transfer coefficient. It was found that the evaporator temperature had little difference under various cooling heat transfer coefficients at a low heat load. For example, at 10 W heating power, the evaporator temperature in all cases was about 35 °C. This was because the heat input to the FLHP can be completely transferred to the cooling side at a low heat load, including air cooling and water cooling. No residual heat was accumulated in the evaporator. With the increase of heat load, the influence of cooling ability on the thermal control of the FLHP was gradually obvious. At this time, the input heat could not be completely transferred under the cooling condition with the lower heat transfer coefficient. The heat accumulated in the FLHP causes its operating temperature to increase continuously. On the other hand, when the heat transfer coefficient of the condenser of the FLHP is high, the heat carried by the vapor

can be released in time. Even the liquid fluid is further cooled to a lower temperature. When the low-temperature liquid fluid flows back to the evaporator, it can absorb more heat to maintain a lower T_e. As a whole, the higher the cooling heat transfer coefficient is, the lower the slope of the curve of the evaporator temperature is, and the higher the heat transfer limit of the FLHP is.

Table 4. Equivalent heat transfer coefficient of the FLHP condenser under different cooling conditions.

Case	Air Flow Rate Q_a (CMH)	Air Velocity v_a (m/s)	Air-Cooling Heat Transfer Coefficient α_a (W/m^2·°C)	Equivalent Heat Transfer Coefficient of the FLHP Condenser α_{hp} (W/m^2·°C)
A-25	25	0.8	22.73	1195.43
A-45	45	1.5	40.61	2087.89
A-60	60	2.0	51.28	2601.66
A-75	75	2.5	60.77	3047.35
A-100	100	3.3	74.17	3659.33
A-130	130	4.2	85.13	4145.39
A-150	150	5.0	97	4657.73
	Water flow rate Q_w (L/min)	Water velocity v_w (m/s)	Water-cooling heat transfer coefficient α_w (W/m^2·°C)	
W-0.5	0.5	0.17	1243.18	6475.75
W-1.0	1.0	0.33	2164.50	8344.64
W-1.5	1.5	0.50	2993.85	9353.67
W-2.0	2.0	0.67	3285.43	9623.20

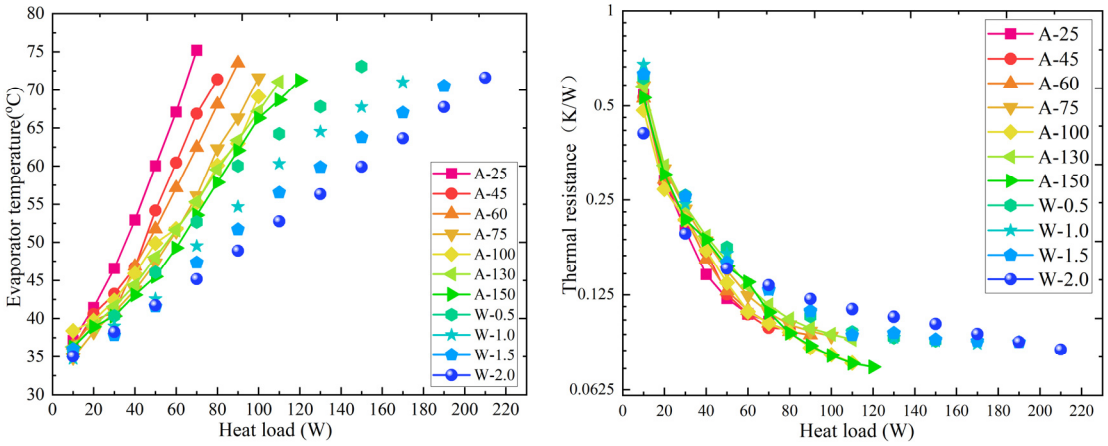

Figure 7. Variation of evaporator temperature and thermal resistance with a heat load under various cooling conditions. (**a**) Evaporator temperature. (**b**) Thermal resistance.

Figure 7b shows the thermal resistance of the FLHP with the increase of heat load at different cooling heat transfer coefficients. As a whole, when the heating power increased, the thermal resistance of the FLHP decreased sharply and tended to level off gradually. This can be attributed to the increase in the circulating rate of working fluid with the increase of thermal load in the FLHP. The working fluid with high-speed circulation can ensure that the surface of the evaporator capillary always keeps a thin liquid layer rather than being submerged by the liquid. As a result, the heat transfer process in the evaporator is at the stage of film evaporation heat transfer. It has a very high heat transfer coefficient, resulting in continued improvements in the thermal performance of the FLHP. In contrast, the thermal resistance of the FLHP was higher at the low heat load stage. The main reason is that the circulation rate is low at this time, resulting in more liquid accumulation in the evaporator. Consequently, the capillary structure of the evaporator is submerged by the

liquid, and the boiling of the liquid needs a higher superheat degree. Therefore, the thermal resistance of the FLHP decreases sharply with the increase in thermal load. According to the experimental results of different cooling conditions, it can be concluded that the FLHP exhibits higher thermal resistance when the cooling heat transfer coefficient is high. This is because the heat carried by the FLHP can be quickly transferred to the external cooling medium when its condenser has a high heat transfer coefficient. Especially at low heat load, the vapor may be condensed into the liquid phase in the front section of the copper tube of the condenser. It is further cooled at the back of the condenser. At this time, the temperature difference in the heat transfer process of the pure liquid phase is very significant, which results in the lower temperature of the working fluid at the outlet of the condenser. Simultaneously, the average temperature at the condenser decreases significantly. According to Formula (2), the thermal resistance of the FLHP is relatively high. In short, if the heat transfer coefficients under different cooling methods are converted into equivalent heat transfer coefficients based on the chip surface area, the maximum equivalent heat transfer coefficients of air cooling, water cooling, and the FLHP are 1415.99 $W/m^2 \cdot °C$, 2727.42 $W/m^2 \cdot °C$ and 3841.48 $W/m^2 \cdot °C$, respectively. Using the FLHP for thermal management of the chip, it can be seen that its heat transfer efficiency is 166 and 41% higher than that of air cooling and water cooling, respectively.

3.2.2. Differences between Air-Cooling and Water-Cooling

In the previous section, the heat transfer principles of the two cooling methods have been analyzed. It is known that the heat transfer of air cooling is realized by the high-speed airflow generated by the fan passing over the fin surface. The heat transfer enhancement method mainly depends on increasing the fin to expand the heat transfer surface area, while the heat in the water cooling method is absorbed and transferred by the liquid flowing in the channel of the cold plate.

After calculating the heat transfer coefficients and the equivalent heat transfer coefficient of the outside tube of the FLHP condenser, it was found that a larger cooling heat transfer coefficient on the FLHP condenser could be easily realized by the water cooling method. For the air cooling method, the rotational speed of the fan needs to be increased to slightly increase its cooling heat transfer coefficient. On the downside, increasing the rotational speed will always bring about a sharp increase in fan power and running noise. It can be seen from Table 4 that the highest air-cooling heat transfer coefficient was 4657.73 $W/m^2 \cdot °C$. As shown in Figure 8, in this case, the maximum heat transfer capacity of the FLHP was 120 W. Accordingly, the power of the fan reached 18 W, which was 15% of the maximum heat transfer power of the FLHP. The noise level reached 59 dB, causing a poor user experience. However, the heat transfer coefficient of water cooling could reach 9623.20 $W/m^2 \cdot °C$ by slightly increasing the pump power to improve the water flow rate. At this time, the maximum heat transfer capacity of the FLHP was increased to 210 W. The pump power was 6 W, which was 2.86% of the maximum heat transfer power of the FLHP, and the noise throughout the cooling system can be ignored. Furthermore, it can be found from Figure 8 that the maximum heat transfer capacity increased linearly with the equivalent heat transfer coefficient. This reflects an essential feature of the FLHP as a heat conduction element. For a particular FLHP, it has a stable heat conduction ability. The maximum heat transfer capacity that can be transferred is mainly determined by the heat digestibility of the cold source side. The FLHP only plays the role of heat transfer; therefore, the increase of the heat transfer coefficient on the cold source side will simultaneously increase the maximum heat transfer capacity of the FLHP.

In addition, the temperature uniformity of the FLHP under two different cooling methods also has great differences. The temperature uniformity can be characterized by the maximum temperature difference on the evaporator surface (ΔT_{max}). ΔT_{max} is defined as the difference between the highest temperature and the lowest temperature among the five temperature measurement points (T_1–T_5) on the evaporator surface when the FLHP is running stably. Figure 9 shows the variation of ΔT_{max} under different operating

conditions. The red curve represents the ΔT_{max} under air-cooling conditions, and the blue point represents that in water-cooling conditions. It can be seen that the water-cooling method is much better than the air-cooling method in controlling temperature uniformity. Before the FLHP reached the heat transfer limit, the temperature difference in the evaporator surface could be kept within 0.5 °C under all water-cooling conditions. Moreover, with the increase of heat load, the increase in temperature difference was slight. By contrast, the maximum temperature difference of the evaporator increased obviously with the increase of heating power when the air-cooling solution was used. What is worse, the maximum temperature difference at the minimum heat load was more than 0.5 °C, and that at the ultimate heat load was over 1.5 °C. The reason for the remarkable difference in the temperature uniformity between the two cooling schemes can be attributed to the difference in the circulating fluency of the working fluid in the FLHP. It is found that the temperature at the outlet of the evaporator is the highest, and the temperature at the inlet is the lowest. For air cooling, the vapor is condensed slowly in the condenser, which leads to a vapor jam at the outlet of the evaporator. So, the temperature near the evaporator outlet is higher. The overall temperature consistency of the evaporator is poor. On the contrary, for water cooling, the circulation of the working fluid is smooth and stable. There will be no vapor blockage and no intermittent backflow of accumulated liquid. Therefore, the temperature uniformity is better.

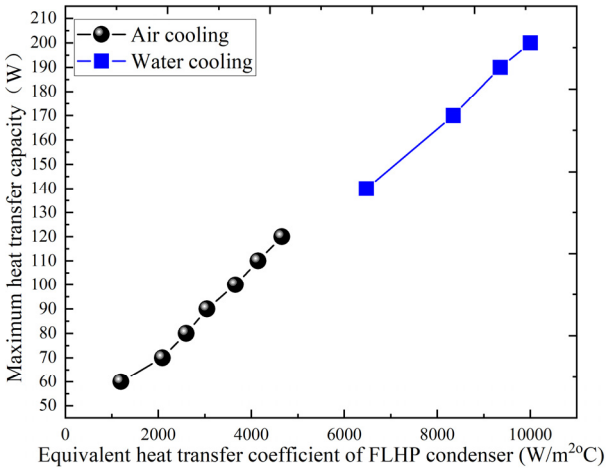

Figure 8. Maximum heat transfer capacity of the FLHP with different cooling methods.

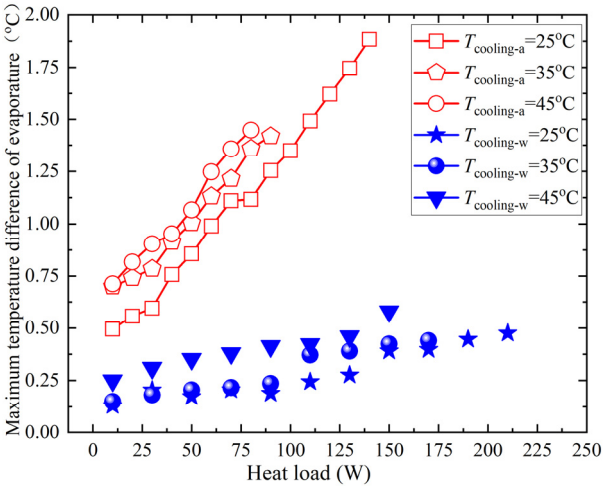

Figure 9. Maximum temperature difference of the evaporator under different cooling conditions.

Last but not least, the start-up performance of the FLHP was also closely related to the cooling mode. Figure 10 shows the temperature changes of the point of T_5 located in the evaporator center during the FLHP start-up process. The red curve and the blue curve represent the air-cooling and water-cooling conditions, respectively. For the two cooling methods, the start-up process of the FLHP was monitored at three cooling temperatures, including 25 °C, 35 °C, and 45 °C. First of all, the higher the cooling temperature is, the higher the start-up temperature of the FLHP is. This means that there must be a certain temperature difference between the evaporator and the condenser to start the FLHP. Only when the pressure difference between the evaporator and the condenser (caused by the vaporization of the liquid medium) is greater than the flow resistance does the working fluid cycle in the heat pipe. The temperature curves under different operating conditions show obvious temperature drop-down intervals. The temperature at the monitoring point first rose sharply, then reached a turning point at 200 s and began to fall sharply. The drop in temperature lasted about 20 s before leveling off. The input heat load of the start-up process was 10 W. Under this low heat load, the pressure difference, which can promote the circulation of the working fluid, cannot be formed quickly due to the less vapor produced. It requires the constant accumulation of vapor, which shows that the evaporator temperature is rising. Until the vapor accumulates enough, it rushes out of the evaporator outlet and flows to the condenser. It releases heat in the condenser and is condensed into a low-temperature liquid. The evaporator temperature will drop significantly as this part of low-temperature fluid comeback. The whole process corresponds to the temperature diving in the start-up curve. Over time, a stream of vapor continuously rushes out of the evaporator and releases heat in the condenser to become a low-temperature condensate. The condensate is recirculated to the evaporator to make a heat balance, and therefore, the temperature curve tends to be stable.

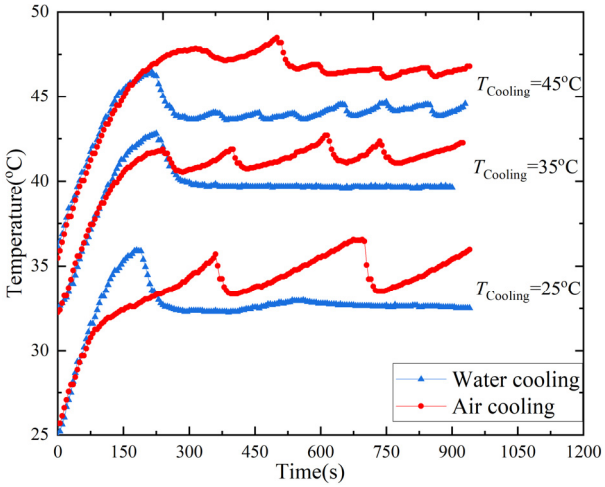

Figure 10. Start-up characteristics of the FLHP under different cooling conditions.

In addition, there were significant differences between the two cooling methods. The drop in temperature of water cooling was larger than that of air cooling. This is because the heat transfer ability of water cooling is stronger than that of air cooling, resulting in lower supercooling of the liquid medium. Furthermore, the temperature fluctuation of the water cooling was smaller after the FLHP start-up, while the air cooling still had an obvious periodic temperature fluctuation. This is because the amount of vapor accumulated was too large, and the cooling ability of air cooling is so poor that it is not possible to condense all the vapor quickly. This causes the vapor to remain in the condenser for a period of time before returning to the evaporator. The cycle of the working fluid was intermittent, and the surface temperature of the evaporator fluctuated periodically. On the contrary, the cooling capacity of water cooling was enough to quickly condense all the vapor flowing to the condenser, ensuring the fluidity of the working fluid cycle. The operating temperature was

very stable. It should be noted that the operating temperature was slightly oscillating when the cooling water temperature was 45 °C. This can be attributed to a decrease in cooling capacity at high water temperatures.

3.2.3. Effect of Water Cooling Temperature

The purpose of cooling the FLHP condenser is to transfer the heat absorbed by the evaporator of the heat pipe to the external environment. This ensures that the heat generated by the heat source with high heat flux can be continuously transferred away by the heat pipe. Different cooling methods will produce different cooling heat transfer coefficients, which are manifested as differences in the cooling capacity of the FLHP. The factor that determines the heat release efficiency of the FLHP condenser is not only the cooling heat transfer coefficient but also the temperature difference between the cooling medium and the heat pipe condenser. Keeping other conditions unchanged, increasing the heat exchange temperature difference of the FLHP condenser by reducing the temperature of the cooling medium can certainly improve its heat exchange ability. However, reducing the cooling temperature comes at a price, such as the energy efficiency of the cooling system. It is relatively easy to properly reduce the cooling temperature within a certain range. If a slight reduction in the cooling temperature can bring about a significant improvement in FLHP performance, this is a very cost-effective solution. But when the cooling medium needs to drop to an extremely low temperature to ensure the operation of the FLHP, the operating cost of the entire cooling system will rise sharply.

Therefore, it is necessary to clarify the relationship between the cooling temperature and the working performance of the FLHP. Based on the previous analysis, water cooling has a much higher heat transfer capacity than air cooling. Next, under the condition of water cooling, the influence of different temperatures of cooling water on the maximum heat transfer capacity, operating temperature, and thermal resistance of the FLHP is mainly explored.

Figure 11a shows the variation of the evaporator temperature with the heat load at different cooling temperatures. It can be seen that the cooling water temperature is positively correlated with the operating temperature of the FLHP. The higher the cooling temperature is, the higher the operating temperature of the FLHP is. The heat dissipation of the FLHP condenser is determined by the temperature of the cooling water. An increase in water temperature will cause a decrease in the temperature difference between the FLHP condenser and the cooling water. As a result, the heat dissipation decreases, which eventually leads to the accumulation of heat at the evaporator of the FLHP. When the cooling temperature increased from 20 °C to 45 °C, the maximum heat transfer capacity of the FLHP decreased from 230 W to 130 W. It can be seen that the cooling temperature has a significant effect on the performance of the FLHP. Based on this conclusion, in the practical application of the FLHP, the most cost-effective cooling temperature can be adopted in combination with the heat generation level of the heat source. Especially in cooling systems that need to use natural cooling sources, a higher cooling temperature can maximize the use of natural cooling sources, thereby reducing system energy consumption.

Figure 11b exhibits the variation of thermal resistance of the FLHP with cooling temperature. The result shows that the thermal resistance of the FLHP is higher at the same heating power when the cooling temperature is lowered. As the temperature of the external cooling fluid decreases, the heat dissipation capacity of the condenser of the FLHP is increased. The vapor may be condensed into a liquid phase in the front section of the copper tube of the condenser, and it is further cooled at the back of the condenser. At this time, the temperature difference in the heat transfer process of the pure liquid phase is very significant, which results in the lower temperature of the working fluid at the outlet of the condenser. This results in an increase in the temperature difference between its evaporator and condenser. Ultimately, it turns out that the thermal resistance of the FLHP increases with decreasing cooling water temperature. Overall, the FLHP exhibited excellent heat transfer efficiency at each cooling temperature tested. The thermal resistance in the

steady state of all cases was below 0.15 K/W. As the heating power increased, the thermal resistance of FLHP decreased continuously, which indicates that the FLHP had not yet reached the capillary limit. Since the FLHP explored in this implementation is used to cool server chips, the upper-temperature limit is controlled at 70 °C. Therefore, the limit of the heat load is taken as the operating condition point where the evaporator temperature reaches 70 °C.

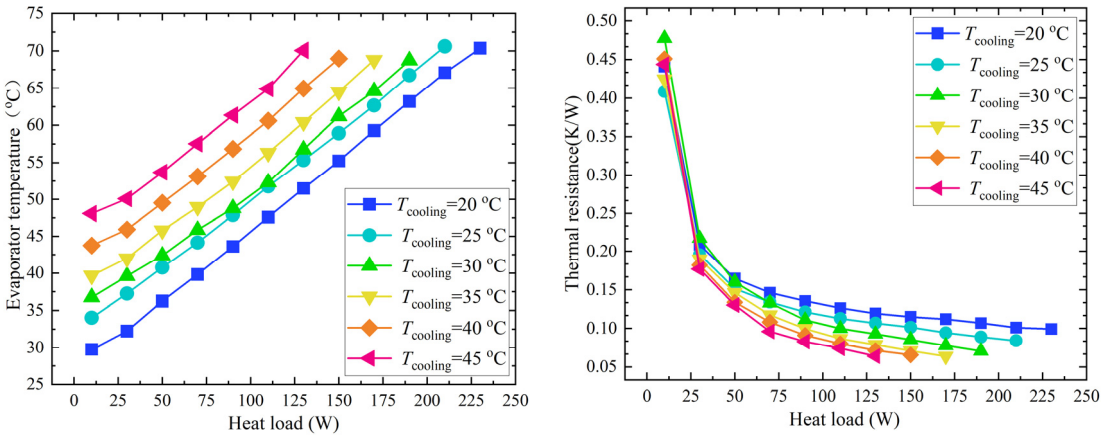

Figure 11. Variation of the evaporator temperature and thermal resistance with a heat load under various cooling temperatures. (**a**) Evaporator temperature. (**b**) Thermal resistance.

4. Conclusions

In this paper, aiming at chip-level cooling solutions for data centers, a FLHP with an evaporator designed with a "Tesla valve" flow channel configuration is proposed. The thermal performance of the FLHP under various installation angles and cooling conditions were experimentally explored. Some main conclusions can be summarized as follow.

(1) When there is a height difference between the FLHP condenser and evaporator, it will facilitate the reflux of working fluid and improve the operating performance of the FLHP. The inclination angle of 20° is the critical point where the effect of gravity on the performance of the FLHP. Below this angle, the assisting effect of gravity is very significant. It can increase the heat load limit of the FLHP from 30 W at 0° to 120 W at 20°. After this critical point, the further increase of gravitational force becomes weaker to promote the circulation of the FLHP working fluid. At this time, it is not the driving force of the working fluid cycle that determines the working performance of the FLHP but the heat dissipation ability at the condenser of the FLHP. The difference in operating temperature of the FLHP after a 20° inclination angle is small.

(2) The cooling heat transfer coefficient at the condenser of the FLHP is the key factor in determining the working performance of the FLHP. The equivalent heat transfer coefficients of the FLHP condenser under different cooling conditions were calculated. It is found that water cooling can provide higher cooling heat transfer coefficients with lower energy consumption and operating noise. In air cooling, the highest equivalent heat transfer coefficient of the FLHP condenser is 4657.73 W/m^2·°C with energy consumption of 18 W and noise of 59 dB. In water cooling, the maximum equivalent heat transfer coefficient is 9623.20 W/m^2·°C with energy consumption of 6 W and negligible noise. The maximum heat transfer capacity of FLHP increase linearly as the cooling heat transfer coefficient increases.

(3) In addition to the difference in the heat transfer coefficient, water cooling can make the FLHP exhibit a more stable start-up performance and higher temperature uniformity than air cooling. Especially at lower cooling temperatures, there is still a temperature fluctuation of 1.5 °C after the FLHP is fully started under air-cooled

conditions. However, water cooling is basically stable in the range of 0.3 °C. In terms of temperature uniformity, water cooling can ensure that the maximum temperature difference on the surface of the evaporator can be controlled within 0.5 °C under all working conditions, while it will exceed 1.5 °C for air cooling.

(4) The factors that determine the heat dissipation on the condensing side of the FLHP mainly include the cooling heat transfer coefficient of the condenser and the temperature of the cooling medium. The heat transfer limit of the FLHP can be significantly increased by reducing the temperature of the cooling water. When the temperature of cooling water drops from 45 °C to 20 °C, the maximum heat transfer capacity of the FLHP increases from 130 W to 230 W. However, reducing the cooling temperature will always sacrifice the energy efficiency of the cooling system, and it is not conducive to the use of natural cooling sources. Therefore, in practical applications, it is necessary to select the most cost-effective cooling temperature based on the actual heating power of the heat source.

Author Contributions: Methodology, Z.L.; Validation, Y.T.; Formal analysis, X.Z.; Investigation, Y.T.; Resources, X.Z.; Data curation, Y.T.; Writing—original draft, Y.T.; Writing—review & editing, Z.L. All authors have read and agreed to the published version of the manuscript.

Funding: This research was funded by [Foshan Shunde District 2020 core technology project] grant number [2030218000156]. And The APC was funded by [Foshan Shunde District 2020 core technology project].

Data Availability Statement: The data that support the findings of this study are available on request from the corresponding author. The data are not publicly available due to privacy.

Conflicts of Interest: The authors declare no conflict of interest.

Nomenclature

A	surface area (mm^2)	*Subscripts*	
d	wire diameter (mm)	a	air
DC	direct current	c	condenser
h	height (mm)	e	evaporator
L	length (mm)	f	fin
m	mass filling of fluid (g)	hp	heat pipe
N	fin number	i	inner
Nu	Nusselt number	max	maximum
Pr	Prandtl number	min	minimum
Q	Volume flowrate (m^3/h or L/min)	o	outer
r	radius (mm)	to	total
R	thermal resistance (K/W)	v	vapor
Re	Reynolds number	w	water
t	thickness (mm)		
T	temperature (K, °C)		
v	velocity (m/s)		
W	width (mm)		
Greek symbols			
α	heat transfer coefficient ($W/m^2 \cdot °C$)		
η	fin surface efficiency (%)		
δ	fin Spacing δ (mm)		
ξ	net face ratio		
ν	kinematic viscosity (m^2/s)		
λ	thermal conductivity ($W/m \cdot °C$)		

References

1. Ichinose, Y.; Hayashi, M.; Nomura, S.; Moser, B.; Hiekata, K. Sustainable Data Centers in Southeast Asia: Offshore, Nearshore, and Onshore Systems for Integrated Data and Power. *Sustain. Cities Soc.* **2022**, *81*, 103867. [CrossRef]
2. Weissberger, A. Synergy Research Group: Hyperscale Data Center Count > 500 as of 3Q-2019. Available online: https://techblog.comsoc.org/2019/10/19/synergy-research-group-hyperscale-data-center-count-500-as-of-3q-2019/ (accessed on 19 October 2019).
3. Andrae, A.S.G. Total Consumer Power Consumption Forecast. Available online: https://10times.com/nordic-digital-businesssummit (accessed on 1 October 2017).
4. Shao, X.; Zhang, Z.; Song, P.; Feng, Y.; Wang, X. A review of energy efficiency evaluation metrics for data centers. *Energy Build.* **2022**, *271*, 112308. [CrossRef]
5. Masanet, E.; Shehabi, A.; Lei, N.; Smith, S.; Koomey, J. Recalibrating global data center energy-use estimates. *Science* **2020**, *367*, 984–986. [CrossRef]
6. Oró, E.; Taddeo, P.; Salom, J. Waste heat recovery from urban air cooled data centres to increase energy efficiency of district heating networks. *Sustain. Cities Soc.* **2019**, *45*, 522–542. [CrossRef]
7. Davies, G.F.; Maidment, G.G.; Tozer, R.M. Using data centres for combined heating and cooling: An investigation for London. *Appl. Therm. Eng.* **2016**, *94*, 296–304. [CrossRef]
8. Greenpeace. Potential Analysis on Energy Consumption of Data Centers and Renewable Energy in China 2019. Available online: https://www.greenpeace.org.cn/china-data-center-electricity-consumption-and-renewable-energy/ (accessed on 9 September 2019).
9. Zhang, H.; Shao, S.; Xu, H.; Zou, H.; Tian, C. Free cooling of data centers: A review. *Renew. Sustain. Energy Rev.* **2014**, *35*, 171–182. [CrossRef]
10. Lim, S.-Y.; Chang, H.-J. Airflow management analysis to suppress data center hot spots. *Build. Environ.* **2021**, *197*, 107843. [CrossRef]
11. Zhang, Y.; Shan, K.; Li, X.; Li, H.; Wang, S. Research and Technologies for next-generation high-temperature data centers—State-of-the-arts and future perspectives. *Renew. Sustain. Energy Rev.* **2023**, *171*, 112991. [CrossRef]
12. Sekiguchi, K.; Waragai, S.; Uekusa, T.; Yamasaki, K. Development of a High-Efficiency Air Cooled Packaged Air-Conditioner for Data Centers. *ASHRAE Trans.* **2010**, *116*, 330–335.
13. Udagawa, Y.; DrEng, K.S.; DrEng, M.Y.; DrEng, T.U.; Naito, Y. Development of an outdoor air cooling-type air-cooled package air conditioner for data centers. *ASHRAE Trans.* **2013**, *119*, 167–175. [CrossRef]
14. Joshi, Y.; Kumar, P. *Energy Efficient Thermal Management of Data Centers*; Springer Science & Business Media: Berlin/Heidelberg, Germany, 2012.
15. Haghshenas, K.; Setz, B.; Bloch, Y.; Aiello, M. Enough Hot Air: The Role of Immersion Cooling. *arXiv* **2022**, arXiv:2205.04257.
16. Beghi, A.; Cecchinato, L.; Mana, G.D.; Lionello, M.; Rampazzo, M.; Sisti, E. Modelling and control of a free cooling system for Data Centers. *Energy Procedia* **2017**, *140*, 447–457. [CrossRef]
17. Ko, J.-S.; Huh, J.-H.; Kim, J.-C. Improvement of Energy Efficiency and Control Performance of Cooling System Fan Applied to Industry 4.0 Data Center. *Electronics* **2019**, *8*, 582. [CrossRef]
18. Saini, M.; Webb, R.L. Heat rejection limits of air cooled plane fin heat sinks for computer cooling. In Proceedings of the ITherm 2002. Eighth Intersociety Conference on Thermal and Thermomechanical Phenomena in Electronic Systems (Cat. No. 02CH37258), San Diego, CA, USA, 30 May–1 June 2002; pp. 1–8.
19. Samadiani, E.; Joshi, Y.; Mistree, F. The Thermal Design of a Next Generation Data Center: A Conceptual Exposition. *J. Electron. Packag.* **2008**, *130*, 041104. [CrossRef]
20. Fan, S.; Duan, F. A review of two-phase submerged boiling in thermal management of electronic cooling. *Int. J. Heat Mass Transf.* **2020**, *150*, 119324. [CrossRef]
21. Ellsworth, M.J., Jr.; Goth, G.F.; Zoodsma, R.J.; Arvelo, A.; Campbell, L.A.; Anderl, W.J. An Overview of the IBM Power 775 Supercomputer Water Cooling System. *J. Electron. Packag.* **2012**, *134*, 020906. [CrossRef]
22. Garimella, S.V.; Yeh, L.T.; Persoons, T. Thermal Management Challenges in Telecommunication Systems and Data Centers. *IEEE Trans. Compon. Packag. Manuf. Technol.* **2012**, *2*, 1307–1316. [CrossRef]
23. Kadam, S.T.; Kumar, R. Twenty first century cooling solution: Microchannel heat sinks. *Int. J. Therm. Sci.* **2014**, *85*, 73–92. [CrossRef]
24. Asadi, M.; Xie, G.; Sunden, B. A review of heat transfer and pressure drop characteristics of single and two-phase microchannels. *Int. J. Heat Mass Transf.* **2014**, *79*, 34–53. [CrossRef]
25. Lee, Y.J.; Singh, P.K.; Lee, P.S. Fluid flow and heat transfer investigations on enhanced microchannel heat sink using oblique fins with parametric study. *Int. J. Heat Mass Transf.* **2015**, *81*, 325–336. [CrossRef]
26. Dede, E.M.; Liu, Y. Experimental and numerical investigation of a multi-pass branching microchannel heat sink. *Appl. Therm. Eng.* **2013**, *55*, 51–60. [CrossRef]
27. Habibi Khalaj, A.; Halgamuge, S.K. A Review on efficient thermal management of air- and liquid-cooled data centers: From chip to the cooling system. *Appl. Energ.* **2017**, *205*, 1165–1188. [CrossRef]
28. Kang, D.; Lee, J.; Chakraborty, A.; Lee, S.-E.; Kim, G.; Yu, C. Recent Advances in Two-Phase Immersion Cooling with Surface Modifications for Thermal Management. *Energies* **2022**, *15*, 1214. [CrossRef]

29. Wu, C.; Tong, W.; Kanbur, B.B.; Duan, F. Full-scale Two-phase Liquid Immersion Cooing Data Center System in Tropical Environment. In Proceedings of the 2019 18th IEEE Intersociety Conference on Thermal and Thermomechanical Phenomena in Electronic Systems (ITherm), Las Vegas, NV, USA, 28–31 May 2019; pp. 703–708.
30. McGlen, R.J.; Jachuck, R.; Lin, S. Integrated thermal management techniques for high power electronic devices. *Appl. Therm. Eng.* **2004**, *24*, 1143–1156. [CrossRef]
31. Yue, C.; Zhang, Q.; Zhai, Z.; Ling, L. Numerical investigation on thermal characteristics and flow distribution of a parallel micro-channel separate heat pipe in data center. *Int. J. Refrig.* **2019**, *98*, 150–160. [CrossRef]
32. Tang, H.; Tang, Y.; Wan, Z.; Li, J.; Yuan, W.; Lu, L.; Li, Y.; Tang, K. Review of applications and developments of ultra-thin micro heat pipes for electronic cooling. *Appl. Energ.* **2018**, *223*, 383–400. [CrossRef]
33. Sohel Murshed, S.M.; Nieto de Castro, C.A. A critical review of traditional and emerging techniques and fluids for electronics cooling. *Renew. Sustain. Energy Rev.* **2017**, *78*, 821–833. [CrossRef]
34. Tang, Y.; Cao, J.; Wang, S. Experimental Research on Thermal Performance of Ultra-Thin Flattened Heat Pipes. *J. Therm. Sci.* **2022**, *31*, 2346–2362. [CrossRef]
35. Tharayil, T.; Asirvatham, L.G.; Ravindran, V.; Wongwises, S. Thermal performance of miniature loop heat pipe with graphene–water nanofluid. *Int. J. Heat Mass Transf.* **2016**, *93*, 957–968. [CrossRef]
36. Gai, D.; Liu, Z.; Liu, W.; Yang, J. Operational characteristics of miniature loop heat pipe with flat evaporator. *Heat Mass Transf.* **2009**, *46*, 267–275. [CrossRef]
37. Zhou, G.; Li, J.; Jia, Z. Power-saving exploration for high-end ultra-slim laptop computers with miniature loop heat pipe cooling module. *Appl. Energy* **2019**, *239*, 859–875. [CrossRef]
38. Zhang, Y.; Luan, T.; Jiang, H.; Liu, J. Visualization study on start-up characteristics of a loop heat pipe with a carbon fiber capillary wick. *Int. J. Heat Mass Transf.* **2021**, *169*, 120940. [CrossRef]
39. Mo, D.; Zou, G.; Lu, S.; Zhang, L.W. A Flow Visualization Study on the Temperature Oscillations Inside a Loop Heat Pipe With Flat Evaporator. In Proceedings of the ASME 2013 International Technical Conference and Exhibition on Packaging and Integration of Electronic and Photonic Microsystems, Burlingame, CA, USA, 16–18 July 2013.
40. Tang, Y.; Hong, S.; Wang, S.; Deng, D. Experimental study on thermal performances of ultra-thin flattened heat pipes. *Int. J. Heat Mass Transf.* **2019**, *134*, 884–894. [CrossRef]
41. Holman, J.P. *Heat Transfer*; China Machine Press: Beijing, China, 2011.